Chondroitin sulfate and caseinophosphopeptides doped polyurethane-based highly porous 3D scaffolds for tendon-to-bone regeneration

International Journal of Pharmaceutics 652 (2024) 123822

Contents lists available at ScienceDirect

International Journal of Pharmaceutics

journal homepage: www.elsevier.com/locate/ijpharm

Chondroitin sulfate and caseinophosphopeptides doped polyurethane-based highly porous 3D scaffolds for tendon-to-bone regeneration

Eleonora Bianchi [a], Marco Ruggeri [a], Elena Del Favero [b], Roberto Pisano [c], Fiora Artusio [c], Caterina Ricci [b], Barbara Vigani [a], Anita Ferraretto [d,e], Cinzia Boselli [a], Antonia Icaro Cornaglia [f], Silvia Rossi [a], Giuseppina Sandri [a,*]

[a] Department of Drug Sciences, University of Pavia, via Taramelli 12, 27100 Pavia, Italy
[b] Department of Medical Biotechnology and Translational Medicine, Università degli Studi di Milano, Milano, Italy
[c] Department of Applied Science and Technology (DISAT), Polytechnic of Torino, Torino, Italy
[d] Department of Biomedical Sciences for Health, Università degli Studi di Milano, via Mangiagalli 31, Milan, Italy
[e] Laboratory of Experimental Biochemistry & Molecular Biology, IRCCS Istituto Galeazzi-Sant'Ambrogio, Via Cristina Belgioioso 173, 20157 Milan, Italy
[f] Department of Public Health, Experimental and Forensic Medicine, University of Pavia, via Forlanini 2, 27100 Pavia, Italy

ARTICLE INFO

Keywords:
Tendon disorders
Thermoplastic polyurethane
Chondroitin sulfate
Caseinophosphopeptides
Mechanical properties
AFM

ABSTRACT

Tendon disorders are common injuries, which can be greatly debilitating as they are often accompanied by great pain and inflammation. Moreover, several problems are also related to the laceration of the tendon-to-bone interface (TBI), a specific region subjected to great mechanical stresses. The techniques used nowadays for the treatment of tendon and TBI injuries often involve surgery. However, one critical aspect of this procedure involves the elevated risk of fail due to the tissues weakening and the postoperative alterations of the normal joint mechanics. Synthetic polymers, such as thermoplastic polyurethane, are of special interest in the tissue engineering field as they allow the production of scaffolds with tunable elastic and mechanical properties, that could guarantee an effective support during the new tissue formation. Based on these premises, the aim of this work was the design and the development of highly porous 3D scaffolds based on thermoplastic polyurethane, and doped with chondroitin sulfate and caseinophosphopeptides, able to mimic the structural, biomechanical, and biochemical functions of the TBI. The obtained scaffolds were characterized by a homogeneous microporous structure, and by a porosity optimal for cell nutrition and migration. They were also characterized by remarkable mechanical properties, reaching values comparable to the ones of the native tendons. The scaffolds promoted the tenocyte adhesion and proliferation when caseinophosphopetides and chondroitin sulfate are present in the 3D structure. In particular, caseinophosphopeptides' optimal concentration for cell proliferation resulted 2.4 mg/mL. Finally, the systems evaluation in vivo demonstrated the scaffolds' safety, since they did not cause any inflammatory effect nor foreign body response, representing interesting platforms for the regeneration of injured TBI.

1. Introduction

Tendons are bridging connective tissues which possess the function of connecting the muscles to bones. In particular, they transmit the mechanical stresses while providing flexibility, enhancing joint stability, and allowing body locomotion (Bianchi et al., 2021, Liu et al., 2008). Tendons owe their remarkable biomechanical properties to the high degree of organization of the extracellular matrix (ECM), which is principally formed by type I collagen and organized in a hierarchical structure of bundles parallel to the long axis (Thorpe, 2016). Moreover, an important region for the tendons functions is represented by the tendon-to-bone interface (TBI), a highly specific region directly connected to the bone where the tendon tissue is gradually reinforced with hydroxyapatite. This complex structure renders the TBI fundamental for the stress concentration reduction, consequently facilitating the transfer between the tendon and the bone (Deymier-Black et al., 2015, Jiang

* Corresponding author.
E-mail address: g.sandri@unipv.it (G. Sandri).

https://doi.org/10.1016/j.ijpharm.2024.123822
Received 14 November 2023; Received in revised form 16 January 2024; Accepted 16 January 2024
Available online 18 January 2024

et al., 2022). The TBI injuries, together with the tendon ones, are considered quite common, resulting in more than 33,000 cases of surgical repair procedures reported annually only in the United States (Liu et al., 2008). Despite the numerous treatment approaches attempted to improve the healing, such as the use of autografts and allografts, the rehabilitation protocol often requires long periods of treatment, also including an elevated risk of fail due to the tissues weakening and the postoperative alterations of the normal joint mechanics (Walden et al., 2017). To overcome these limitations, polymers-based scaffolds have been proposed in tendon tissue engineering to replace and restore the tissue, mimicking the structural, biomechanical, and biochemical functions of the tendon extracellular matrix (Bianchi et al., 2021). In particular, synthetic polymers are of great interest in the tissue engineering field, since they could facilitate the production of versatile scaffolds with controlled mechanical properties, consequently assuring the support of the mechanical stresses during the new tissue formation (Janoušková, 2018). This aspect is of fundamental importance in the development of orthopaedic scaffolds, since the implants need to significantly withstand to repeated cycles of mechanical loads (Ambrose, 2015, Al-Shalawi et al., 2023, Figueiredo et al., 2020).

Currently, a major part of orthopaedic implants should be removed after the tendon/ligament recovery. Moreover, the innovative resorbable materials most studied nowadays in orthopaedic tissue engineering, such as polyethylene, polylactide (both in D and L isoforms), and polyglycolide, are characterized by a mechanical stiffness too low for the effective mimicking of the aimed tissue, fundamental to induce the mechanotransduction of cell response (Kennedy et al., 2017, Kumbar et al., 2014). They also resulted to cause disadvantageous responses of the tissues, such as foreign body reaction (Matsuda et al., 2021, Yolcu et al., 2015). For these reasons, synthetic polymers as medical grade thermoplastic polyurethane (TPU) represent an interesting alternative, thanks to their controlled mechanical properties, blood compatibility and resistance to microorganisms (Bergmeister et al., 2013, Korthagen et al., 2019, Wendels and Avérous, 2021).

TPUs are a widely used polymer class in various biomedical applications, such as catheters and prosthetic heart valve leaflets, as they possess excellent mechanical properties and biocompatibility (Pedicini and Farris, 2003). Moreover, they are susceptible to hydrolytic, oxidative and enzymatic degradation in vivo, resulting an interesting tool to design biodegradable scaffolds (Chen et al., 2010, Tatai et al., 2007).

However, the hydrophobic nature of TPU could represent an impediment for the cell adhesion and proliferation onto the scaffolds, consequently blocking the production of new ECM and the tissue reconstruction (Jasmee et al., 2018). In order to stimulate the cell anchorage and overcome the problems related to TPU hydrophobicity, in this work an innovative approach has been studied by investigating the addition of caseinophosphopeptides (CPPs) into the porous structure of the polymeric scaffolds.

In particular, the addition of CPPs has been evaluated due to the lack of a suitable biointerface between the tendon scaffold and the insertion with the bone, which could lead to a poor and insufficient TBI healing. In fact, the scaffolds could require up to 3 years to sufficiently integrate with the host bone, resulting as the limiting factor for a safe and successful tissue healing (Lin et al., 2019, Han et al., 2015, Ekdahl et al., 2008, Park et al., 2001).

At this purpose, the combination of the highly porous scaffolds with CPPs, which are phosphorylated peptides enzymatically released from casein after in vitro and in vivo digestion, provides an interesting approach for the TBI regeneration since they were proven to promote calcium uptake, due to their cation-binding activity, and osteoblast differentiation (Perego et al., 2015, Donida et al., 2009). Moreover, chondroitin sulfate (CS) has been added into the polymeric matrix, since it is a glycosaminoglycan (a structural component of the ECM) able to interact with positively charged bioactive molecules, such as growth factors, resulting effective in the cell proliferation enhancement and wound healing (Sandri et al., 2019, Saporito et al., 2018).

Given these premises, the aim of this work was the design and development of highly porous 3D scaffolds based on TPU, doped with CS, and thereafter enriched with CPPs, in order to mimic the tissue mechanical performance and enhance the healing potential. These are intended to be resorbable, in order to prevent second surgeries intended to remove the implant (Ambrose, 2015, Al-Shalawi et al., 2023, Figueiredo et al., 2020,).

2. Materials and methods

2.1. Materials

Medical-grade thermoplastic polyurethane (TPU) (Pathway^{TM}, PY-PT83AE100 aliphatic polyether, Lubrizol Advanced Materials, New Milford, USA); chondroitin sulfate (CS) (β-1,4-linked d-glucuronic acid and β-1,3-linked N-acetyl galactosamine) bovine 100 EP, low Mw 14 kDa, mixture of chondroitin A (chondroitin 4 sulfate) and chondroitin C (chondroitin 6 sulfate) (Bioiberica, Barenz, Italy); CPP CE90CPP enzymatically hydrolyzed casein (DMV International, Delhi, New York) purity 26 % (w/w).

2.2. Preparation of the polymeric blends

TPU was dissolved in water:acetic acid (1:9 vol ratio) under magnetic stirring overnight at room temperature. Two different TPU percentages (8 % and 10 % w/w) were used in order to evaluate the influence of the polymer concentration on the systems morphology and porosity, obtaining two different scaffolds, namely T8 and T10. Both blends were afterwards enriched with 1 % w/w of CS, obtaining two more scaffolds, namely T8-CS and T10-CS.

2.3. Preparation of the highly porous scaffolds

The polymeric blends were withdrawn in rectangular molds (dimensions: 6 × 2 cm; for each mold, 4 mL of blend were used). These were then frozen at – 20 °C for 12 h and freeze-dried for 72 h at 0.020 mbar (Heto Drywinner sublimator, Analitica De Mori, Italy) in order to allow the complete sublimation of the solvent and obtain sponge-like systems. The scaffolds were insoluble in water.

2.4. Scaffolds physico-chemical characterization

The scaffolds morphology was assessed by means of scanning electron microscope (SEM) analysis (Tescan, Mira3XMU, Brno, Czech Republich). The samples were cut in pieces (dimensions: 5 × 5 mm) and put onto stubs using a dedicated double-sided tape, then they were sputtered with 20 nm of graphite. The scaffolds pores area (μm^2) and porosity (%) were assessed by image analysis software (ImageJ, ICY, Institut Pasteur, Paris, France). Moreover, the scaffolds morphology and profilometry was also assessed by means of Atomic Force Microscopy (AFM, Tosca 200 Anton Paar, Austria) in Tapping Mode (cantilever AP-ARROW-NCR, Silicon SPM-Sensor, Al-coating; thickness: 4.6 μm, Length: 160 μm, width: 45 μm, resonance frequency: 285 kHz, force constant: 42 N/m; Anton Paar, Austria). Also for AFM, the samples were cut in pieces (dimensions: 5 × 5 mm) and put onto the sample holder using a dedicated double-sided tape.

The wettability of the scaffolds was tested by contact angle measurements (DMe-211 Plus; FAMAS software, Kyowa, Osaka, Japan), after 1, 5, and 10 s of contact of a PBS droplet (1.4 μL volume) with the scaffolds surface.

2.5. Structural characterization

Small Angle X-ray Scattering analysis was performed using synchrotron light at the ID02 SAXS beamline of ESRF (Grenoble, France), (https://doi.org/10.15151/ESRF-ES-58593). Small pieces of scaffolds

(0.5 x 0.5 cm) were cut, inserted in Kapton capillaries and fully hydrated with water. The scattered intensity was measured in a wide range of momentum transfer q $0.006 < q < 6$ nm^{-1}, where $q = 4\pi se(\vartheta/2)/\lambda$, being ϑ the scattering angle and $\lambda = 0.1$ nm the x-ray wavelength. The intensity spectra were acquired at two different sample-to-detector distances, namely 1 m and 10 m, and joined after angular regrouping.

2.6. Mechanical properties evaluation

The mechanical properties of the scaffolds were measured using a dynamometer (TA-XT plus, Stable Microsystems, Italy) equipped with a 5.0 kg load cell. Before testing, the scaffolds were cut 30 × 10 mm and the strips (thickness range: 0.9–1.1 mm) were clamped between two tensile grips (A/TG probe) setting an initial distance between the grips of 10 mm. Then, the upper grip was moved forward at a constant speed of 5.0 mm/s up to break. Mechanical properties were evaluated both in dry and hydrated state, and force at break vs. distance was recorded. The stress–strain curves and the scaffolds' Young's Modulus (YM) were calculated as follows:

$$Stress = \frac{F}{A}$$

Where F is the applied force and A is the cross-sectional area of the sample's analyzed area

$$Strain = \frac{L_f - L_0}{L_0}$$

Where L_f is the final length and L_0 is the initial length of the sample's analyzed area

$$YM = \frac{Stress}{Strain}$$

The YM of the scaffolds in the nanoscale was assessed by means of Atomic Force Microscopy (AFM, Tosca 200 Anton Paar, Austria) in Contact Mode (cantilever AP-ARROW-CONTR-10, Silicon SPM-Sensor, Al-coating; thickness: 2 μm, Length: 450 μm, width: 45 μm, resonance frequency: 14 kHz, force constant: 0.2 N/m; Anton Paar, Austria).

An analysis of the morphology during stimulation to mechanical stresses was also performed by SAXS. The samples were cut into rectangular strips of about 1 by 6 cm and mounted directly on the x-ray beamline, as shown in Figure S1 (Supplementary Information), with a distance between the grips of 3.5 at rest. Measurements were performed at different elongations $\Delta l/l = 0$, 0.33, 0.66, 0.83. The scattered intensity was acquired on a 2D detector and visualized to observe asymmetries in the pattern both in dry and wet conditions.

2.7. CPPs and CS release

The release of CS from the scaffolds was assayed using a CS ELISA kit (Aviva Systems Biology, San Diego, USA) for quantitative measurement of CS. The scaffolds (dimensions: 30 × 10 mm, weight: 100 mg) were put at 37 °C in 2 mL of PBS (phosphate-buffered saline pH 7.4, Sigma-Aldrich, Milan, Italy). Supernatants were collected after 7, 14, and 21 days, and the CS content was evaluated at 450 nm, setting 570 nm as wavelength correction. The method was linear with concentrations from 3 to 0.06 mg/mL, having an R^2 of 0.9992. T8 and T10 scaffolds were used as negative control.

For the evaluation of the CPPs release from the scaffolds, CPPs at different concentrations (2.4 mg/mL, 3.2 mg/mL, 6.4 mg/mL) were suspended in the cell medium (tenocyte growth medium (ZenBio, Durham, USA) supplemented with 10 % v/v fetal bovine serum (FBS, Euroclone, Milan, Italy) and with 200 IU/mL penicillin/0.2 mg/mL streptomycin (Sigma-Aldrich, Milan, Italy), as described in section 2.8) and then put in contact with the scaffolds in order to allow the complete CPPs adsorption into the porous structure. The scaffolds were then put at 37 °C in 2 mL of PBS. The supernatants collected after 7, 14, and 21 days were analysed by means of Bradford assay (Bradford reagent, Sigma-Aldrich, St. Louis, MO, USA). 5 μL of samples were put in contact with 250 μL of the Bradford reagent for 45 min, and the reaction was evaluated at 595 nm. The method was linear with concentrations from 6.5 to 0.06 mg/mL, having an R^2 of 0.9997.

2.8. Cell proliferation assay

Proliferation and cell viability were carried out using normal human tenocytes (TEN-1) (1st–5th passages, ZenBio, Durham, NC, USA). TEN-1 were cultured in collagen (rat tail collagen coating solution, Cell Applications, Italy) coated flasks, using tenocyte growth medium (ZenBio, Durham, USA) supplemented with 10 % v/v fetal bovine serum (FBS, Euroclone, Milan, Italy) and with 200 IU/mL penicillin/0.2 mg/mL streptomycin (Sigma-Aldrich, Milan, Italy). They were grown into an incubator (CO_2 Incubator, PBI International, Milano, Italy) at 37 °C in a 5 % CO_2 atmosphere with 95 % relative humidity (RH).

Each scaffold (5 mm diameters, 0.2 mm thickness) was sterilized by UV radiation for 15 min and placed in a 96-well plate to perfectly cover the bottom.

CPPs at different concentrations (2.4 mg/mL, 3.2 mg/mL, 6.4 mg/mL) were suspended in the cell medium and then put in contact with the scaffolds in order to allow the complete CPPs adsorption into the porous structure. At this point, TEN-1 were seeded onto the scaffolds at a density of $2x10^4$ cells/well density and re-incubated. Scaffolds without CPPs were also tested. TEN-1 grown in standard conditions (growth medium, GM) with and without contact with CPPs suspension were considered as control. After 7, 14, and 21 days of contact with the scaffolds, the medium was removed and 10 % (v/v) Alamar Blue (AlamarBlue HS cell viability reagent, Invitrogen, Thermo Fisher, Monza, Italy) was diluted with the appropriate medium and added in the wells (100 μL). After 3 h of incubation in dark at 37 °C, the Alamar Blue solution was collected from the wells and transferred in a new plate. Each well was then refilled with the culture medium and left in culture again. Alamar Blue fluorescence was recorded using a microplate reader (FLUOstar® Omega, BMG LABTECH, Aylesbury, UK) with λex = 530 nm and λem = 590 nm. Cell viability was expressed as fluorescence intensity (FI).

2.9. Cell morphology

The cell morphology after 21 days of contact with the scaffolds was investigated using CLSM after nuclei and cytoskeleton staining. Cells grown onto the scaffolds were fixed using a 3 % (v/v) glutaraldehyde solution in PBS for 2 h at room temperature. The substrates were then washed three times with PBS. Cellular cytoskeleton was stained with FITC Atto 488 phalloidin (green, Sigma-Aldrich, Milan, Italy; 50 μL at 20 μg/mL in PBS in each well, contact time 40 min), and the cell nuclei were then stained with propidium iodide (red, Sigma-Aldrich, Milano, Italy; 50 μL/sample at 25 μg/mL in PBS in each well, contact time 2 min). Scaffolds were placed onto microscope slides and imaged using a Confocal Laser Scanning Microscope (CLSM, Leica TCS SP2, Leica Microsystems, Buccinasco (MI), Italy) with λex = 535 nm and λem = 617 nm for propidium iodide, and λex = 501 nm and λem = 523 nm for FITC-phalloidin. The acquired images were processed with a software (Leica Microsystem, Buccinasco (MI), Italy).

2.10. In vivo evaluation of systems safety

All animal experiments were carried out in full compliance with the standard international ethical guidelines (European Communities Council Directive 2010/63/EU) approved by Italian Health Ministry (D. L. 116/92). The study protocol was approved by the Local Institutional Ethics Committee of the University of Pavia for the use of animals and by ISS (Istituto Superiore di Sanità). 9 male rats (Wistar rats with a weight

between 200 and 250 g, Envigo RMS S. r.L.) were anesthetized with equitensine at 3 mL/kg and shaved to remove all hair from their backs. All animals were monitored for the following 3 days by animal care. Scaffolds were cut and subcutaneously implanted as described in a previous work (Bianchi et al., 2023a). 18 days after the treatment, full thickness biopsies were taken, and the histological analysis performed. A biopsy of intact skin was also taken for comparison as a control.

2.10.1. Histological analysis

As described in a previous work (Bianchi et al., 2023a), the tissue samples were immediately immersed in 4 % v/v neutral buffered formalin and embedded in paraffin. One group of samples was stained with hematoxylin and eosin (H&E), whereas the other with picrosirius red (PSR). In order to apply PSR deparaffinized sections were hydrated, stained with Weigert's hematoxylin for nuclei, and afterwards stained with PSR for 1 h. After the staining, the sections were observed using a light microscope (Carl Zeiss Axiophot) and imaged (Nikon DS-Fi2).

2.11. Statistical analysis

Statistical analyses were performed using Astatsa statistical calculator. One-way analysis of variance (ANOVA) was followed by Scheffé for post-hoc comparisons. $p < 0.05$ was considered significant.

3. Results and discussion

3.1. Scaffolds physico-chemical characterization

The scaffolds' porous structure is a fundamental parameter to guide and promote the formation of the new tissue. In fact, the porosity could facilitate the diffusion of nutrients and waste materials, consequently affecting the cell migration, proliferation, and differentiation. In literature, numerous studies are reported on how the scaffolds pore area and porosity shows a direct effect on the functionality, affecting cell nutrition, proliferation, and migration for tissue vascularization and formation of new tissues (Kim et al., 2019, Yadav et al., 2021). In particular, it has been shown that the amount of extracellular matrix produced together with the amount of glycosaminoglycans secretion, and the expression of collagen gene markers is affected by the pore size of the scaffolds, showing a preferential proliferation when the pore area is between 250 and 500 μm^2 (Lien et al., 2009), and this could be easily characterized using Image analysis that was correlated in different studies with other methodologies, resulting reliable (Calore et al., 2023, Tuan Ho and Hutmacher, 2006). Moreover, porosity and interconnectivity at around 80 % also facilitate cell migration within the porous structure, stimulating cell growth and avoiding cell aggregation and overcrowding (Loh and Choong, 2013). At this purpose, T10 and T10-CS scaffolds possess an optimal and homogeneous microporous structure (as shown in Fig. 1a, where the SEM micrographs are reported), since they are characterized by a pore area of 352.40 ± 63.70 μm^2 and 399.33 ± 89.54 μm^2 respectively, and a porosity of 72.29 ± 5.09 % and 75.44 ± 8.21 % respectively. On the other hand, T8 and T8-CS scaffolds are characterized by larger pores (2924.99 ± 789.81 μm^2 and 2524.55 ± 802.01 μm^2 respectively) and a lower porosity (16.41 ± 2.09 % and 16.92 ± 1.60 % respectively), which could result in cell aggregation and inhibition of the cell nutrition (as shown in Fig. 1b, where the pore area (μm^2) and the porosity (%) are reported).

In Fig. 1c, AFM images and the corresponding profiles as height (μm) vs length (μm) are reported. These results confirm that the scaffolds topography is formed by a rough surface and the scale of the z-direction height changes on the microscale as the SEM micrographs suggest.

Fig. 1d reports the shape and the contact angle values of a buffer droplet released onto the scaffolds' surface. It is evident that the presence of CS is effective in improving the systems wettability. Moreover, the contact angle values confirm the scaffolds' porosity. In fact, T10 and T10-CS, which are characterized by the best porosity, also show lower contact angle values. More importantly, after 10 s of contact the droplet is almost completely adsorbed into the structure, while after 10 s of contact with T8 and T8-CS the droplet stays onto the surface. This confirms both the higher porosity of T10 and T10-CS, and the effectiveness of the CS incorporation into the structure as hydrophilic component. In fact, also T8-CS is characterized by a lower contact angle than T8, despite the similar porosity. Previous studies confirm that the incorporation of hydrophilic compounds leads to the increase of the surface wettability, which is crucial for appropriate cell adhesion and is manifested by the decrease in the contact angle measurement from 86°, typical of pure TPU, to 78° or less (Naureen et al., 2021).

3.2. Structural characterization

Small angle x-ray scattering (SAXS) experiments were carried out on the highly porous scaffolds to investigate their structure on the nanoscale. Fig. 2 reports the scattering profiles of T8, T8-CS, T10 and T10-CS scaffolds in hydrated conditions.

Spectra show many common features. First, in the low-q region the intensity decays follow a double power-law slope, $I(q) \div q\text{-}s$, with an exponent $3.7 < s < 4$ in the region $q < 0.04\ nm^{-1}$, corresponding to lengths > 150 nm, characteristic of surface fractal structures, with low to negligible roughness. The second slope, with $s = -2.8$, is observed in the region $0.04 < q < 0.2\ nm^{-1}$, corresponding to lengths in the range 30–150 nm. This decay behavior is characteristic of the mass fractal arrangement of TPU in the porous matrix.

Second, in all spectra, a broad peak at $q = 0.7\ nm^{-1}$, corresponding to a characteristic distance $d = 9$ nm, and a small peak at $q = 1.4\ nm^{-1}$ are observed. The presence of these peaks confirms the known inhomogeneous structure of TPU on the nanoscale, with a nanophase-separated arrangement of soft and hard domains (Sui et al., 2019, Javni et al., 2015).

Doping with CS does not affect dramatically the internal arrangement of scaffolds. In T8-CS differences can be observed in the high-q region of the spectra (nm length-scale), where the intensity profile follows a $q^{-1.7}$ power law, characteristic of polymer chains in a good solvent, which could protrude from the surface in hydrated conditions. In T10-CS this behaviour is less pronounced, suggesting that CS chains could have been more homogeneously distributed in the TPU fibrous matrix. These results furtherly prove that CS is deeply entangled in the polymeric matrix structure, as already suggested by the contact angle measurement, resulting in a more suitable surface for cell adhesion and proliferation.

3.3. Mechanical properties evaluation

It is known that the scaffolds mechanical properties could be important to affect cell differentiation and regenerative functions, since the mechanical properties of the ECM environment have the capability to influence intracellular signalling and cell response (Hastings et al., 2019). The mechanical properties of the scaffolds were assessed by means of tensile measurement and nanomechanics, and the structural evolution upon tension was investigated using SAXS. Fig. 3 reports the mechanical properties (a: maximum force at break, Fmax; b: elongation %; c: YM calculated by stress–strain curves) of highly porous scaffolds both in dry and hydrated state, while Fig. 3d reports the YM evaluated with the nanomechanics. The scaffolds' stress–strain curves were also recorded and reported in Figure S2 (Supplementary Information). As a general trend the scaffolds based on the 10 % of TPU (T10 and T10-CS) are characterized by remarkable mechanical properties, higher than T8 and T8-CS scaffolds. In fact, they are able to stand higher stresses and larger deformation before breaking. Moreover, the presence of CS into the polymer structure seems to increase both the Fmax and elongation % of the scaffolds. However, the differences between T8 and T8-CS, and between T10 and T10-CS are not significant. This means that the CS probably reinforces the structure acting as doping into the polymeric

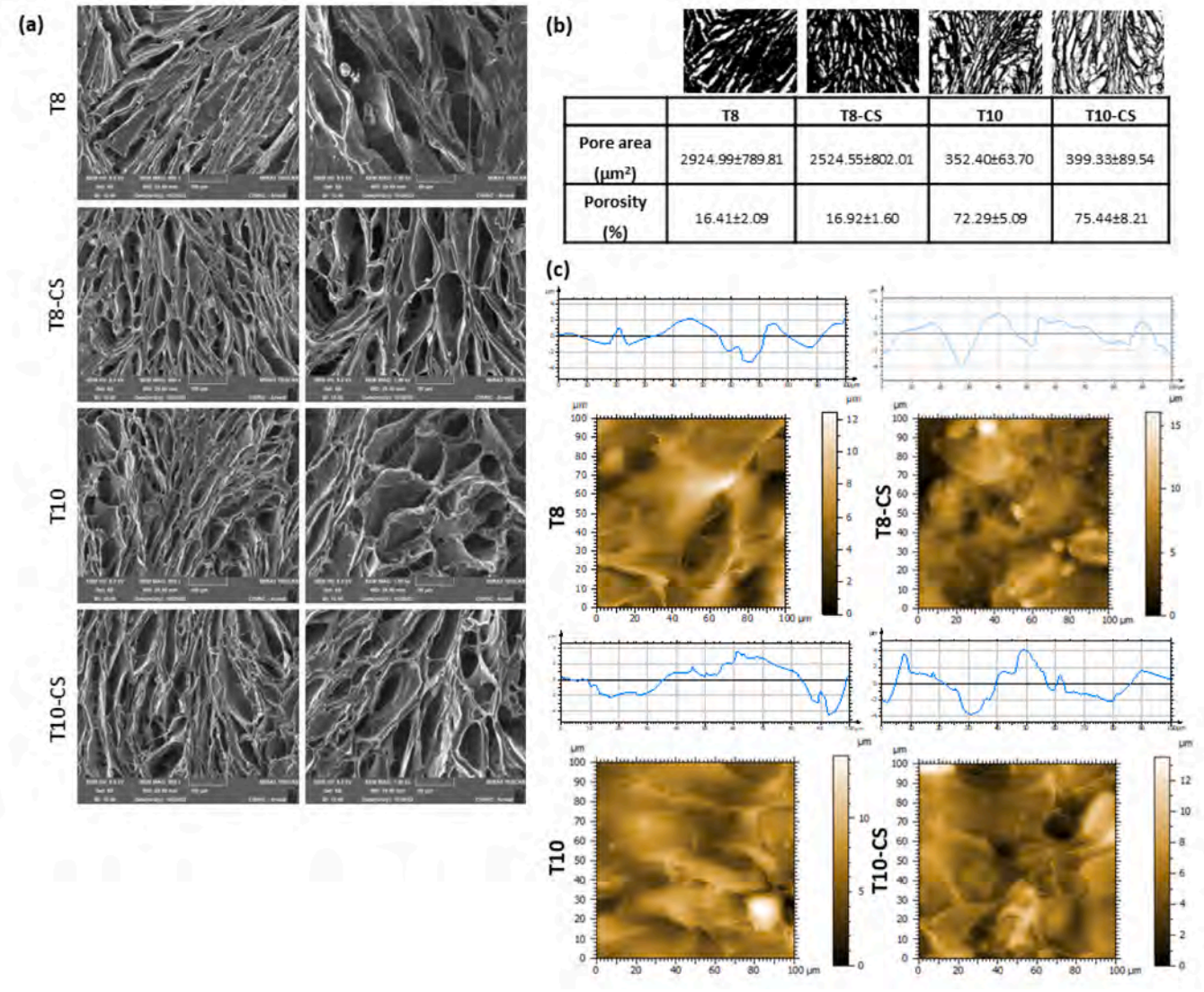

	T8	T8-CS	T10	T10-CS
Pore area (μm²)	2924.99±789.81	2524.55±802.01	352.40±63.70	399.33±89.54
Porosity (%)	16.41±2.09	16.92±1.60	72.29±5.09	75.44±8.21

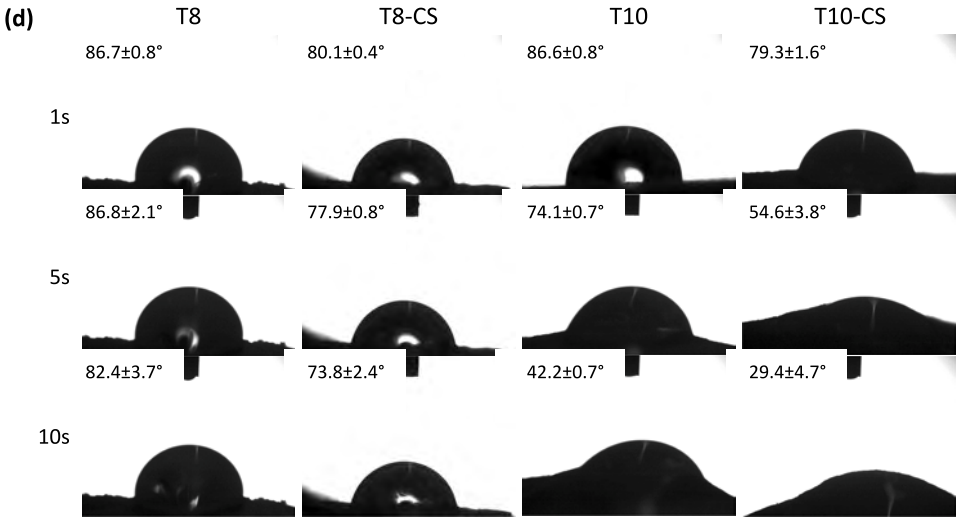

Fig. 1. (a) SEM micrographs of T8, T8-CS, T10, and T10-CS at 500 x and 1.00kx magnifications; (b) pore area (μm^2) and porosity (%) of the scaffolds with the corresponding binary image of the porosity (mean values ± s.d.; n = 30). ANOVA one-way; Scheffé test ($p < 0.01$): T8 vs T10, T10-CS; T8-CS vs T10, T10-CS.; (c) AFM morphological images of T8, T8-CS, T10, and T10-CS scaffolds with the corresponding profilometry (scan area 100 × 100 μm^2); (d) images of the buffer after 1, 5, and 10 s of contact with the scaffolds' surface. In each image, the contact angle value is reported (mean values ± s.d.; n = 5) (needle diameter = 0.405 mm). ANOVA one-way; Scheffé test ($p < 0.01$): T8 vs T10, T10-CS; T8-CS vs T10, T10-CS.

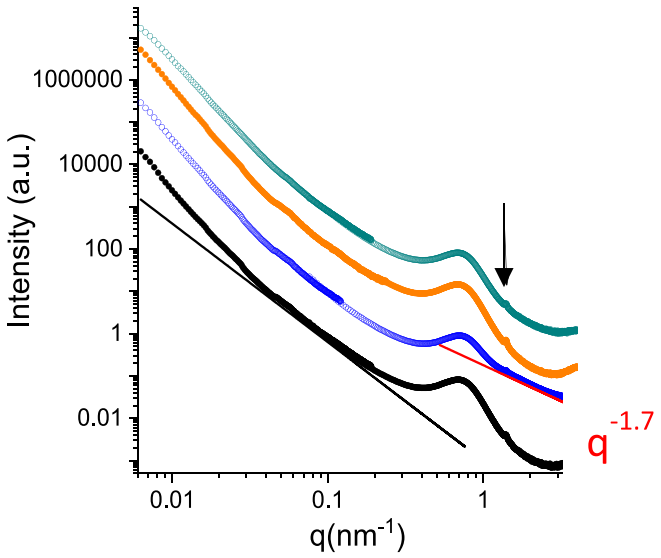

Fig. 2. SAXS spectra of T8, T8-CS, T10 and T10-CS highly porous scaffolds vertically shifted for better visibility. Lines represent the trend of the I(q) decay. The arrow indicates the small peak at q = 1.4 nm^{-1}.

chains, but the mechanical properties are mainly related to the scaffolds' morphology and porosity. In fact, the large pore area of T8 and T8-CS scaffolds leads to a larger amount of void volume into the structure, consequently compromising the mechanical properties (Loh and Choong, 2013, Karageorgiou and Kaplan, 2005). Noticeably, the T10 and T10-CS scaffolds mechanical properties mimic the ones of the native tendons, which vary accordingly to their location with an ultimate tensile strength that ranges from 5 to 100 MPa (Lim et al., 2019). Moreover, TPU is considered as a resilient elastomer and an excellent candidate to build shape-memory scaffolds with the ability to recover their original shape after being subjected to mechanical stresses until they break (Ahmad et al., 2012). In fact, all scaffolds result able to return to their original shape after mechanical tests when breaking does not occur. This is due to the hard segments of the TPU chains, which serve as physical cross-links and prevent the chains slip from each other when subjected to deformation, acting as a fixed phase during the shape recovery process (Coleman et al., 1986). T10, T10-CS, and T8-CS scaffolds are characterized by remarkable YM values of 213.95 MPa, 249.76 MPa, and 225.17 MPa respectively, while T8 is characterized by a YM of 120.34 MPa (Fig. 3c). This is probably due to the presence of CS that acts as reinforcement by contributing to the polymer chains organization. Moreover, as already mentioned, this is also related to the scaffolds' porosity, as the large pores of T8 compromise its mechanical properties. Interestingly, the YM results from the tensile test largely differ from the YM obtained by AFM nanomechanical evaluation (Fig. 3d). In fact, nanomechanics analysis highlights that T10 and T10-CS scaffolds possess a YM of 197.07 MPa and 756.76 MPa respectively, while T8 and T8-CS possess a YM of 16.11 MPa and 23.26 MPa respectively. This could be due to the scaffold's 3D structure. In fact, the large voids found in T8, and T8-CS could modify the structure's mechanical properties on the nanoscale, rendering the structure more sensitive to deformation upon stress applied with respect to T10 and T10-CS, that are characterized by a total polymer concentration. The scaffolds' capability to stand great mechanical stresses in the nanoscale is fundamental to better lead to the stimulation of cells guidance and proliferation (Zhou et al.,

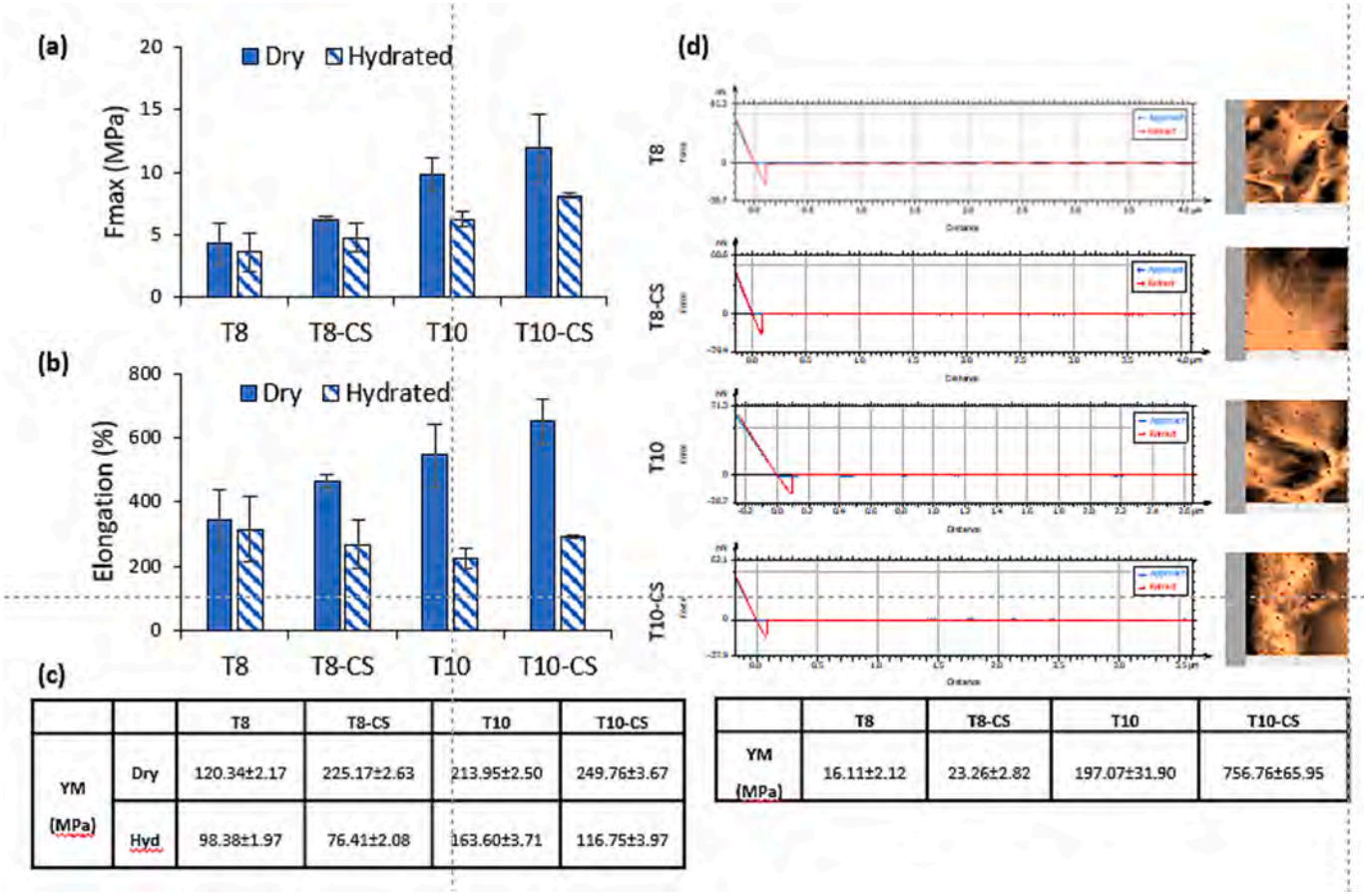

(c)

		T8	T8-CS	T10	T10-CS
YM (MPa)	Dry	120.34±2.17	225.17±2.63	213.95±2.50	249.76±3.67
	Hyd	98.38±1.97	76.41±2.08	163.60±3.71	116.75±3.97

	T8	T8-CS	T10	T10-CS
YM (MPa)	16.11±2.12	23.26±2.82	197.07±31.90	756.76±65.95

Fig. 3. (a) Fmax (MPa), (b) elongation %, (c) YM calculated with the tensile test, and (d) YM determined by AFM with corresponding maps and modulus profiles (mean values ± s.d.; n = 10).

2021, Kilpatrick et al., 2015). On this base, mechanical tests highlight that T10 and T10-CS structures seem more suitable than T8 and T8-CS for the cell homing and to organize the newly formed collagen to restore native tendons.

To investigate the evolution of the nanoscale structure while the scaffolds were subjected to elongation, SAXS experiments were carried out on scaffolds under tension. A rectangular (1x6 cm) sample was mounted in a mechanical stretcher, with 3 cm in length at rest, subjected to an in situ elongation sequence along the stretcher axis. The scattered X-ray pattern was collected on a 2D detector at each consecutive strain increment $\Delta l/l = 0$, 0.33, 0.66, 0.83. Fig. 4 reports the 2D patterns collected for the different TPU samples in dry conditions. As a function of strain, patterns became asymmetric, evolving from circular to elliptical with a shrinkage in the meridional direction, along the stretcher axis, and an expansion in the equatorial direction, perpendicular to the stretcher axis. The preferential orientation, as expected, became aligned with the elongation axis, i.e., the short axis of the elliptical pattern in reciprocal space (I(q)) corresponding to longer distances in real space. At constant deformation, the scattering pattern did not display any evolution during the short acquisitions (1 s), as in the case of negligible viscous effects. Also, the symmetry of the scattering patterns recovered when the systems were unloaded.

The intensity profiles on the meridional and equatorial directions have been extracted for each system both at rest and at 0.66 strain. Results are reported in Figure S3 (Supplementary Information). At rest the I(q) profiles are almost superimposable, while they differ under tension. The calculated parameters to regain the overlap of meridional and equatorial profiles to the ones at rest can give information on the effective structural changes on the nanoscale when the TPU scaffolds were submitted to macroscopic elongation. Results on the calculated strains along the elongation axis are reported in Table 1, compared with the imposed macroscopic strain. Interestingly the values of nano-scale

Table 1
Macroscopic strain as imposed by the mechanical stretcher $\varepsilon_{macro} = \Delta l/l$, nanoscopic strain along the elongation axis ε_{nano} in dry and hydrated conditions.

Blend	ε_{macro}	ε_{nano} dry	ε_{nano} hydrated
T8	0.66	0.66	0.42
T8-CS	0.66	0.42	0.42
T10	0.66	0.42	0.25
T10-CS	0.66	0.25	0.25

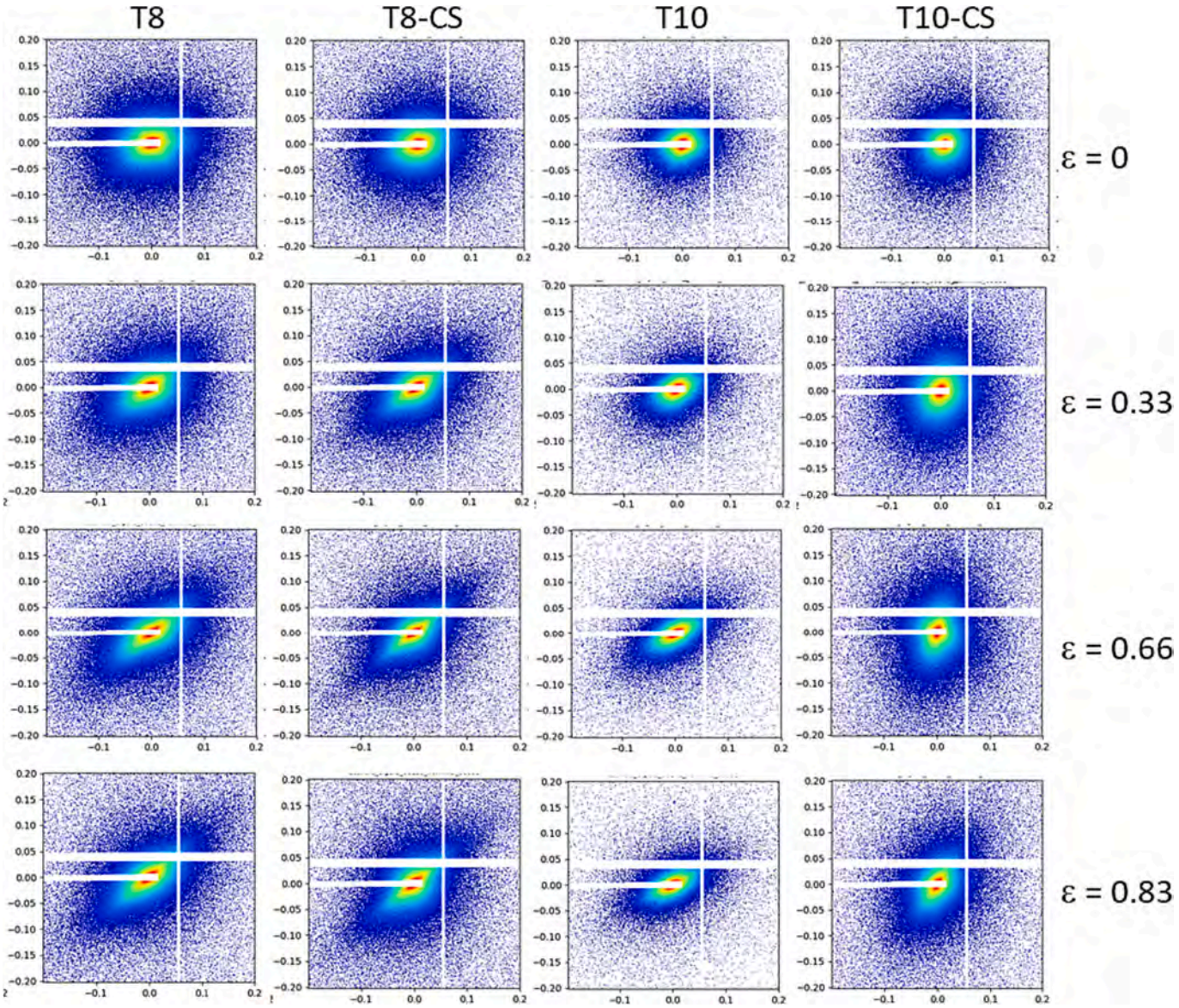

Fig. 4. Scattering intensity 2D patterns for T8, T8-CS, T10 and T10-CS scaffolds at different elongations.

elastic strains are lower than the macro-scale ones. Results indicate that the porous TPU matrix does not simply deform under tension, but rearranges itself, deforming locally less than expected. This rearrangement is made possible by the peculiar structure of TPU, constituted of polydisperse hard and soft domains and crystallites, affecting its mechanical properties, as already observed for different TPU systems (Stribeck et al., 2011, Sui et al., 2015).

Both the concentration of TPU and the presence of CS favored the adaptability of the structure. Moreover, this behavior is confirmed even in hydrated conditions. The ratio between the SAXS-derived nano-scale strain to the macroscopic strain is about 0.38 for T10 and T10-CS in the hydrated state along the elongation axis. This deformation inhomogeneity across the scales can favor in vivo cell adhesion and proliferation when the scaffold is subjected to the same stress conditions as the tendon.

3.4. CPPs and CS release

The evaluation of the CPPs release (Fig. 5a) shows that the CPPs adsorbed are released over time from the scaffolds, reaching a complete

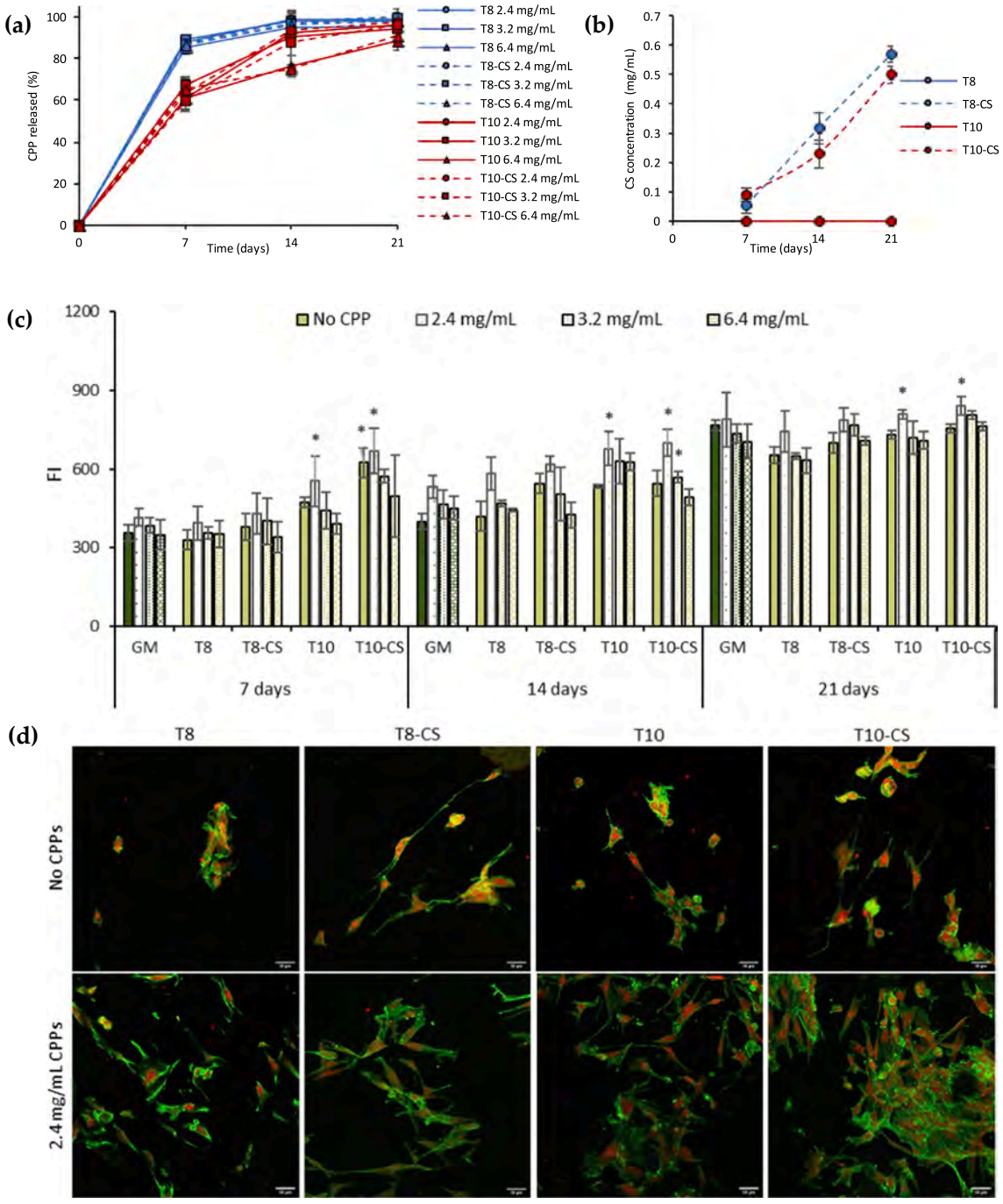

Fig. 5. (a) CPP release (%) from the scaffolds at different time intervals (mean values ± s.d.; n = 4); (b) CS release from T8-CS and T10-CS scaffolds at different time intervals (mean values ± s.d.; n = 6); (c) Alamar blue assay evaluated for T8, T8-CS, T10 and T10-CS scaffolds without CPPs adsorption and with different CPPs concentrations adsorption (2.4 mg/mL, 3.2 mg/mL, and 6.4 mg/mL); (d) CLSM images of TEN-1 grown onto the scaffolds after 21 days of culture. Nuclei stained in red, cytoskeleton stained in green (scale bar: 50 μm) (mean values ± s.d.; n = 6). * indicates statistical differences with the positive control (GM). (For interpretation of the references to colour in this figure legend, the reader is referred to the web version of this article.)

release after 21 days. In particular, T8 and T8-CS scaffolds are characterized by a faster CPPs release, showing the values of 87.8 % and 87.3 %, respectively after 7 days, while T10 and T10-CS are characterized by a slower and constant release in 21 days. This could be related to the porosity and the pore area of the scaffolds: T10 and T10-CS are characterized by optimal properties with high porosity and adequate pore surface area, while T8 and T8-CS scaffolds possess a low porosity and a high pore area, that could speed up the CPPs release.

As regards the CS release, Fig. 5b shows that a low amount of CS is slowly released from the scaffolds over time. In particular, T8-CS and T10-CS scaffolds are characterized by a CS release of about 1.4 % and 1.2 % respectively after 21 days. This could be related to the loss of CS that remained on the surface of the scaffolds, which could also lead to a higher cell adhesion and proliferation. On the other hand, this result also suggests that the component is well integrated into the polymeric matrix, consequently being independent of porosity and pore size as suggested by the SAXS investigation (Fig. 2).

3.5. Cell proliferation assay and cell morphology

Proliferation and cell viability were carried out using TEN-1 as representatives for tendon cells in view of the application of the scaffolds in the repair of the tendon interface. Fig. 5c reports the results in fluorescence intensity (FI) of the Alamar blue assay, performed after 7, 14, and 21 days of TEN-1 culture with and without CPPs adsorption into the porous matrices. Cells growth in standard conditions (GM) with and without contact with CPPs suspension at different concentrations (2.4 mg/mL, 3.2 mg/mL, 6.4 mg/mL) were considered as control.

T10 and T10-CS scaffolds are characterized by a cell growth significantly higher than that of the control (cells growth in standard conditions) at every time interval. This could be reconducted to the scaffolds' better morphology and porosity, which facilitate the transport of nutrients and oxygens in vitro, enabling better cell proliferation. Notably, the presence of CS lead to a cell growth higher than the scaffolds of TPU alone. In fact, CS is known as a facilitator of cell adhesion and as an enhancer of proliferation, since it is a type of glycosaminoglycan (GAG) abundantly found among other GAG in the body (Yudistira et al., 2020, Ryan et al., 2015). Moreover, the presence of CPPs in the 2.4 mg/mL concentration significantly increases the cell proliferation higher than the other concentrations, which show a proliferation similar to that of the GM. Since 2.4 mg/mL was the concentration of CPPs that allows the cell proliferation enhancement, TEN-1 adhesion onto the scaffolds was evaluated after 21 days of culture using CLSM and compared to the cells adhered onto the scaffolds without CPPs adsorption (Fig. 5d). The cells adhere preferably onto the T10 and T10-CS scaffolds. Moreover, CPPs adsorption leads to an increase in cell adhesion onto all the scaffolds, and in particular onto the T10 and T10-CS scaffolds, which are highly populated by TEN-1 elongated cells. This also confirms the CPPs capability to affect cell growth through their interaction with ion channels, such as L-type calcium channels and TRPV6 channel, both recognized to exert an active role in calcium absorption, consequently regulating cell proliferation (Perego et al., 2015).

3.6. In vivo evaluation of systems safety

Since T10 and T10-CS were characterized by the best morphology, mechanical properties and cell adhesion and proliferation, they were selected as the optimal scaffolds. The in vivo safety of the scaffolds was investigated in a murine excisional model. A biopsy of intact skin (Fig. 6a) and of the wound treated with saline solution (Fig. 6b) were also taken as positive controls.

After 18 days of treatment no trace of the device is visible and no sign of inflammatory process is recognizable, with no leukocyte recruitment neither foreign body response. In particular, in subcutaneous implant of the scaffolds with CPPs (Fig. 6e and 6f) the implant area is similar to the adjacent control skin and collagen fibers are also restored. T10-CPPs (Fig. 6e) shows a small area of 1.5 μm with granulation tissue and neoangiogenesis without skin appendages in correspondence to the implant, together with an area of new collagen not yet orderly organized, and T10 and T10-CS implants (Fig. 6c and 6d respectively) show a small area that is still in remodeling, although completely regenerated in correspondence of the implant. On the other hand, the presence of CS and CPPs (T10-CS-CPPs, Fig. 6f) in the structure does not even leave any sign of the surgery used for the scaffold implant: the synergic effect of CPPs together with the CS capability of proliferation enhancement allow the better tolerability (Bianchi et al., 2023b).

4. Conclusions

Highly porous 3D scaffolds based on TPU and enriched with CS were successfully manufactured. It was possible to obtain scaffolds with a homogeneous microporous structure, and a 70 % porosity optimal for cell nutrition, proliferation, migration, and for tissue vascularization and new tissues formation.

The observed structure of TPU scaffolds at the nanoscale, with a nanophase-separated arrangement of soft and hard domains, confers peculiar multi-scale mechanical properties to the highly porous scaffolds. On the macroscopic length scale, T10 and T10-CS scaffolds are characterized by remarkable mechanical properties, reaching values comparable to the ones of the native tendons. Moreover, they are able to stand higher stresses than T8 and T8-CS scaffolds, which are characterized by a larger amount of void volume into the structure.

Notably, on the nanoscale, scaffolds submitted to tensile strength display a lower strain than the macroscopic strain along the elongation axis. This different response on different length scales to deformation can promote cell adhesion and proliferation on the scaffolds submitted to mechanical stresses, as during in vivo tendon regeneration. The scaffolds promote the cell adhesion and proliferation, in particular when 2.4 mg/mL of CPPs are adsorbed into the porous structure. Moreover, the CS leads to an increase in the TEN-1 adhesion and proliferation. Finally, the systems in vivo do not cause any inflammatory effect, neither leukocyte recruitment nor foreign body response.

These results highlighted the capability of the systems in mimicking the tissue mechanical properties. More importantly, the CPPs adsorption into the scaffolds highly porous structure evidenced their effectiveness in overcoming the problems related to the TPU hydrophobicity, since they notably increased the cell adhesion and proliferation into the structures.

In conclusion, scaffolds based on TPU and enriched with CS and CPPs deserve particular attention as enhancers of the tendon tissue regeneration and supporters of the mechanical loads during the new tissue formation. Further investigation on the scaffolds efficacy in vivo will assess their capability on augmenting the tendon ECM reconstruction, and eventually speed up their translation to the clinic.

Funding

This research did not receive any specific grant from funding agencies in the public, commercial, or not-for-profit sectors.

CRediT authorship contribution statement

Eleonora Bianchi: Conceptualization, Methodology, Formal analysis, Investigation, Data curation, Writing – original draft, Writing – review & editing, Validation. **Marco Ruggeri:** Investigation. **Elena Del Favero:** Writing – review & editing, Investigation, Formal analysis. **Roberto Pisano:** Methodology. **Fiora Artusio:** Investigation. **Caterina Ricci:** Investigation. **Barbara Vigani:** Visualization, Software. **Anita Ferraretto:** Resources. **Cinzia Boselli:** Investigation. **Antonia Icaro Cornaglia:** Investigation. **Silvia Rossi:** Resources, Funding acquisition. **Giuseppina Sandri:** Conceptualization, Resources, Writing – original draft, Writing – review & editing, Supervision, Project administration, Funding acquisition.

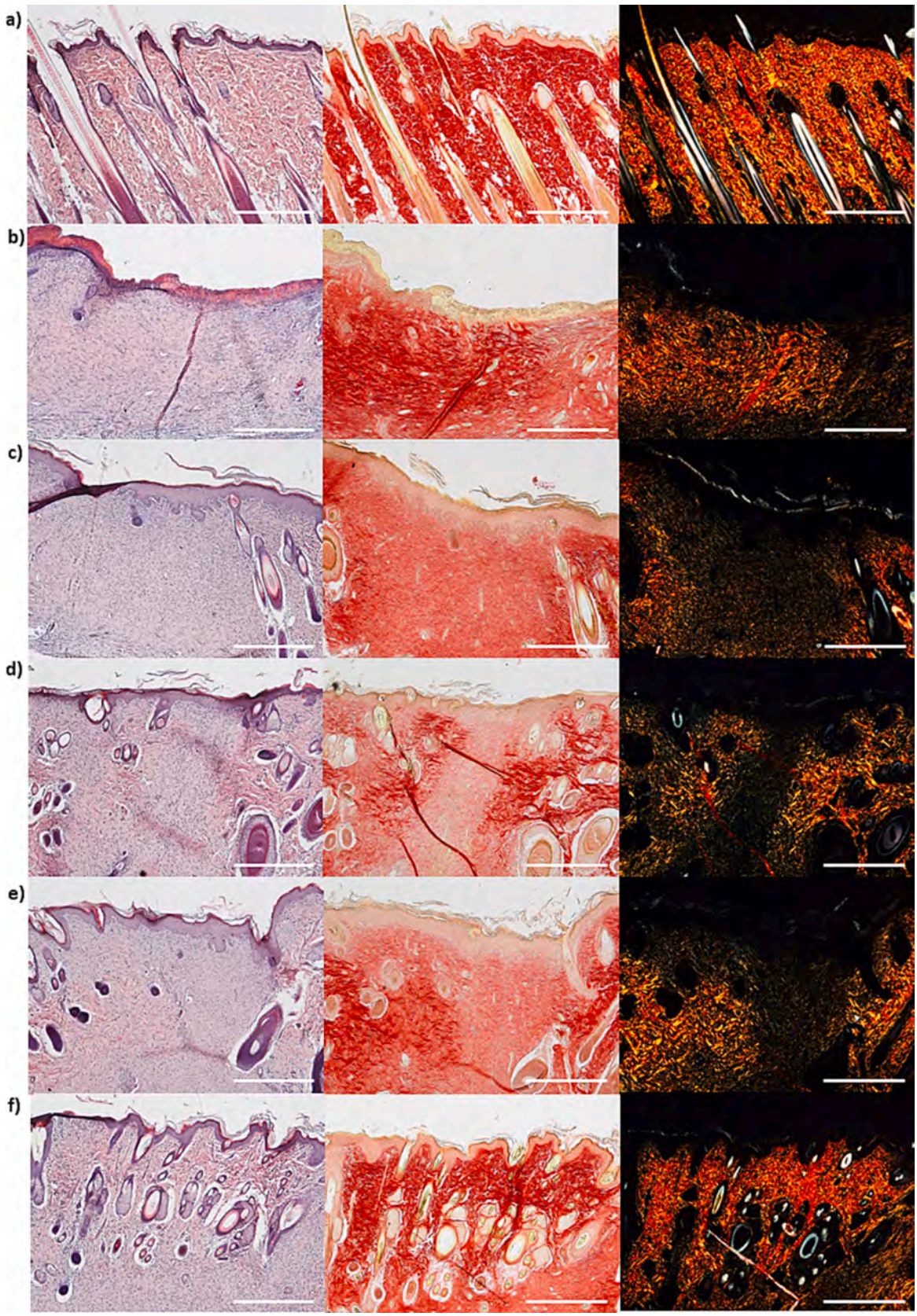

Fig. 6. H&E and PSR sections of (a) intact skin, (b) wound treated with saline solution, (c) subcutaneous implant of T10 scaffold, (d) subcutaneous implant of T10-CS scaffold, (e) subcutaneous implant of T10 with 2.4 mg/mL CPPs adsorption scaffold, (f) subcutaneous implant of T10-CS with 2.4 mg/mL CPPs adsorption scaffold. Original magnification: 5 ×. Each micrograph frame has a width of 1780 μm (scale bar: 500 μm).

Declaration of competing interest

The authors declare that they have no known competing financial interests or personal relationships that could have appeared to influence the work reported in this paper.

Data availability

The authors are unable or have chosen not to specify which data has been used.

Acknowledgments

The authors acknowledge ESRF (Grenoble, Fr) for beamtime allocation and financial support for x-ray experiments (ESRF2021-SC5178) and ID02 staff for precious technical assistance. The authors also acknowledge the animal facility "Centro di servizio per la gestione unificata delle attività di stabulazione e di radiobiologia" of the University of Pavia (Italy) to host the animals and the OPBA of the University of Pavia for support in animal protocol drawing up.

Appendix A. Supplementary data

Supplementary data to this article can be found online at https://doi.org/10.1016/j.ijpharm.2024.123822.

References

Ahmad, M., Xu, B., Purnawali, H., Fu, Y., Huang, W., Miraftab, M., Luo, J., 2012. High Performance Shape Memory Polyurethane Synthesized with High Molecular Weight Polyol as the Soft Segment. Appl Sci 2, 535–548. https://doi.org/10.3390/app2020535.

Al-Shalawi, F.D., Azmah Hanim, M.A., Ariffin, M.K.A., Seng Kim, C.L., Brabazon, D., Calin, R., Al-Osaimi, M.O., 2023. Biodegradable synthetic polymer in orthopaedic application: A review. Mater. Today: Proc. 74, 540–546. https://doi.org/10.1016/j.matpr.2022.12.254.

Ambrose, C.G., Hartline, B.E., Clanton, T.O., Lowe, W.R., McGarvey, W.C., 2015. Polymers in Orthopaedic Surgery, in: Puoci, F. (eds) Advanced Polymers in Medicine. Springer, Cham. Doi: 10.1007/978-3-319-12478-0_5.

Bergmeister, H., Schreiber, C., Grasl, C., Walter, I., Plasenzotti, R., Stoiber, M., Schima, H., 2013. Healing characteristics of electrospun polyurethane grafts with various porosities. Acta Biomater. 9, 6032–6040. https://doi.org/10.1016/j.actbio.2012.12.009.

Bianchi, E., Ruggeri, M., Rossi, S., Vigani, B., Miele, D., Bonferoni, M.C., Sandri, G., Ferrari, F., 2021. Innovative Strategies in Tendon Tissue Engineering. Pharmaceutics 13, 89. https://doi.org/10.3390/pharmaceutics13010089.

Bianchi, E., Ruggeri, M., Vigani, B., Del Favero, E., Ricci, C., Boselli, C., Icaro Cornaglia, A., Viseras, C., Rossi, S., Sandri, G., 2023. Cerium Oxide and Chondroitin Sulfate Doped Polyurethane Scaffold to Bridge Tendons. ACS Appl. Mater. Interfaces 15, 26510–26524. https://doi.org/10.1021/acsami.3c06144.

Bianchi, E., Vigani, B., Ruggeri, M., Del Favero, E., Ricci, C., Grisoli, P., Ferraretto, A., Rossi, S., Viseras, C., Sandri, G., 2023. Electrospun Scaffolds Based on Poly(butyl cyanoacrylate) for Tendon Tissue Engineering. Int. J. Mol. Sci. 24, 3172. https://doi.org/10.3390/ijms24043172.

Calore, A.R., Srinivas, V., Groenendijk, L., Serafim, A., Stancu, I.C., Wilbers, A., Leoné, N., Albillos Sanchez, A., Auhl, D., Mota, C., Bernaerts, K., Harings, J.A.W., Moroni, L., 2023. Manufacturing of scaffolds with interconnected internal open porosity and surface roughness. Acta Biomater 156, 158–176. https://doi.org/10.1016/j.actbio.2022.07.017.

Chen, R., Huang, C., Ke, Q., He, C., Wang, H., Mo, X., 2010. Preparation and characterization of coaxial electrospun thermoplastic polyurethane/collagen compound nanofibers for tissue engineering applications. Colloids Surf B Biointerfaces 79, 315–325. https://doi.org/10.1016/j.colsurfb.2010.03.043.

Coleman, M.M., Lee, K.H., Skrovanek, D.J., Painter, P.C., 1986. Hydrogen bonding in polymers. 4. Infrared temperature studies of a simple polyurethane. Macromolecules 19, 2149–2157. https://doi.org/10.1021/ma00162a008.

Deymier-Black, A.C., Pasteris, J.D., Genin, G.M., Thomopoulos, S., 2015. Allometry of the Tendon Enthesis: Mechanisms of Load Transfer Between Tendon and Bone. J Biomech Eng 137, 11. https://doi.org/10.1115/1.4031571.

Donida, B.M., Mrak, E., Gravaghi, C., Villa, I., Cosentino, S., Zacchi, E., Perego, S., Rubinacci, A., Fiorilli, A., Tettamanti, G., Ferraretto, A., 2009. Casein phosphopeptides promote calcium uptake and modulate the differentiation pathway in human primary osteoblast-like cells. Peptides 30, 2233–2241. https://doi.org/10.1016/j.peptides.2009.08.003.

Ekdahl, M., Wang, J.H., Ronga, M., Fu, F.H., 2008. Graft healing in anterior cruciate ligament reconstruction. Knee Surg Sports Traumatol Arthrosc 16, 935–947. https://doi.org/10.1007/s00167-008-0584-018633596.

Figueiredo, L., Fonseca, R., Pinto, L.F.V., Castelo Ferreira, F., Almeida, A., Rodrigues, A., 2020. Strategy to improve the mechanical properties of bioabsorbable materials based on chitosan for orthopedic fixation applications. J Mech Behav Biomed Mater 103. https://doi.org/10.1016/j.jmbbm.2019.103572.

Han, F., Zhang, P., Sun, Y., Lin, C., Zhao, P., Chen, J., 2015. Hydroxyapatite-doped polycaprolactone nanofiber membrane improves tendon-bone interface healing for anterior cruciate ligament reconstruction. Int J Nanomed 10, 7333–7343. https://doi.org/10.2147/IJN.S9209926677323.

Hastings, J.F., Skhinas, J.N., Fey, D., Croucher, D.R., Cox, T.R., 2019. The extracellular matrix as a key regulator of intracellular signalling networks. Br J Pharmacol 176, 82–92. https://doi.org/10.1111/bph.14195.

Janoušková, O., 2018. Synthetic polymer scaffolds for soft tissue engineering. Physiol Res 67, S335–S348. https://doi.org/10.33549/physiolres.933983.

Jasmee, S., Omar, G., Masripan, N.A.B., Kamarolzaman, A.A., Ashikin, A.S., Che Ani, F., 2018. Hydrophobicity performance of polyethylene terephthalate (PET) and thermoplastic polyurethane (TPU) with thermal effect. Mater Res Express 5. https://doi.org/10.1088/2053-1591/aad81e.

Javni, I., Bilić, O., Bilić, N., Petrović, Z.S., Eastwood, E.A., Zhang, F., Ilavský, J., 2015. Thermoplastic polyurethanes with isosorbide chain extender. J Appl Polym Sci 132. https://doi.org/10.1002/app.42830.

Jiang, X., Kong, Y., Kuss, M., Weisenburger, J., Haider, H., Harms, R., Shi, W., Liu, B., Xue, W., Dong, J., Xie, J., Streubel, P., Duan, B., 2022. 3D bioprinting of multilayered scaffolds with spatially differentiated ADMSCs for rotator cuff tendon-to-bone interface regeneration. Appl Mater Today 27. https://doi.org/10.1016/j.apmt.2022.101510.

Karageorgiou, V., Kaplan, D., 2005. Porosity of 3D biomaterial scaffolds and osteogenesis. Biomaterials 26, 5474–5491. https://doi.org/10.1016/j.biomaterials.2005.02.002.

Kennedy, K.M., Bhaw-Luximon, A., Jhurry, D., 2017. Cell-matrix mechanical interaction in electrospun polymeric scaffolds for tissue engineering: Implications for scaffold design and performance. Acta Biomater. 50, 41–55. https://doi.org/10.1016/j.actbio.2016.12.034.

Kilpatrick, J.I., Revenko, I., Rodriguez, B.J., 2015. Nanomechanics of Cells and Biomaterials Studied by Atomic Force Microscopy. Adv. Healthc. Mater. 4, 2456–2474. https://doi.org/10.1002/adhm.201500229.

Kim, T.R., Kim, M.S., Goh, T.S., Lee, J.S., Kim, Y.H., Yoon, S.Y., Lee, C.S., 2019. Evaluation of Structural and Mechanical Properties of Porous Artificial Bone Scaffolds Fabricated via Advanced TBA-Based Freeze-Gel Casting Technique. Appl. Sci. 9, 1–17. https://doi.org/10.3390/app9091965.

Korthagen, N.M., Brommer, H., Hermsen, G., Plomp, S.G.M., Melsom, G., Coeleveld, K., Mastbergen, S.C., Weinans, H., van Buul, W., van Weeren, P.R., 2019. A short-term evaluation of a thermoplastic polyurethane implant for osteochondral defect repair in an equine model. Vet. J. 251 https://doi.org/10.1016/j.tvjl.2019.105340.

Kumbar, S., Laurencin, C., Deng, M., Eds. Natural and Synthetic Biomedical Polymers, 1st edition. Newnes, (2014).

Lien, S.M., Ko, L.Y., Huang, T.J., 2009. Effect of pore size on ECM secretion and cell growth in gelatin scaffold for articular cartilage tissue engineering. Acta Biomater 5, 670. https://doi.org/10.1016/j.actbio.2008.09.020.

Lim, W.L., Liau, L.L., Ng, M.H., Chowdhury, S.R., Law, J.X., 2019. Current Progress in Tendon and Ligament Tissue Engineering. Tissue Eng. Regen. Med. 16, 549–571. https://doi.org/10.1007/s13770-019-00196-w.

Lin, Y., Zhang, L., Liu, N.Q., Yao, Q., Van Handel, B., Xu, Y., Wang, C., Evseenko, D., Wang, L., 2019. In vitro behavior of tendon stem/progenitor cells on bioactive electrospun nanofiber membranes for tendon-bone tissue engineering applications. Int J Nanomed 14, 5831–5848. https://doi.org/10.2147/IJN.S210509.

Liu, Y., Ramanath, H.S., Wang, D.-A., 2008. Tendon tissue engineering using scaffold enhancing strategies. Trends Biotechnol 26, 201–209. https://doi.org/10.1016/j.tibtech.2008.01.003.

Loh, Q.L., Choong, C., 2013. Three-dimensional scaffolds for tissue engineering applications: role of porosity and pore size. Tissue Eng Part B Rev 19, 485–502. https://doi.org/10.1089/ten.TEB.2012.0437.

Matsuda, Y., Karino, M., Okui, T., Kanno, T., 2021. Complications of Poly-l-Lactic Acid and Polyglycolic Acid (PLLA/PGA) Osteosynthesis Systems for Maxillofacial Surgery: A Retrospective Clinical Investigation. Polymers (basel) 13, 889. https://doi.org/10.3390/polym13060889.

Naureen, B., Haseeb, A.S.M.A., Basirun, W.J., Muhamad, F., 2021. Recent advances in tissue engineering scaffolds based on polyurethane and modified polyurethane. Mater. Sci. Eng. C 118. https://doi.org/10.1016/j.msec.2020.111228.

Park, S.H., Lee, M.C., Seong, S.C., 2001. A comparative study of the healing of tendon autograft and tendon-bone autograft using patellar tendon in rabbits. Int Orthop 25, 35–39. https://doi.org/10.1007/s002640000019911374265.

Pedicini, A., Farris, R.J., 2003. Mechanical behavior of electrospun polyurethane. Polymer 44, 6857–6862. https://doi.org/10.1016/j.polymer.2003.08.040.

Perego, S., Del Favero, E., De luca, P., Dal Piaz, F., Fiorilli, A., Cantù, L., Ferraretto, A., 2015. Calcium bioaccessibility and uptake by human intestinal like cells following in vitro digestion of casein phosphopeptide–calcium aggregates. Food Funct. 6, 1796–1807. https://doi.org/10.1039/c4fo00672k.

Ryan, C.N.M., Sorushanova, A., Lomas, A.J., Mullen, A.M., Pandit, A., Zeugolis, D.I., 2015. Glycosaminoglycans in Tendon Physiology, Pathophysiology, and Therapy. Bioconjug. Chem. 26, 1237–1251. https://doi.org/10.1021/acs.bioconjchem.5b00091.

Sandri, G., Rossi, S., Bonferoni, M.C., Miele, D., Faccendini, A., Del Favero, E., Di Cola, E., Icaro Cornaglia, A., Boselli, C., Luxbacher, T., Malavasi, L., Cantù, L., 2019. Chitosan/glycosaminoglycan scaffolds for skin reparation. Carbohyd. Polym. 220, 219–227. https://doi.org/10.1016/j.carbpol.2019.05.069.

Saporito, F., Sandri, G., Rossi, S., Bonferoni, M.V., Riva, F., Malavasi, L., Caramella, C., Ferrari, F., 2018. Freeze dried chitosan acetate dressings with glycosaminoglycans and traxenamic acid. Carbohydr Polym. 15, 408–417. https://doi.org/10.1016/j.carbpol.2017.12.066.

Stribeck, N., Zeinolebadi, A., Sari, M.G., Frick, A., Mikoszek, M., Botta, S., 2011. Structure and Mechanical Properties of an Injection-Molded Thermoplastic Polyurethane as a Function of Melt Temperature. Macromol Chem Phys 212, 2234–2248. https://doi.org/10.1002/macp.201100193.

Sui, T., Baimpas, N., Dolbnya, I., Prisacariu, C., Korsunsky, A.M., 2015. Multiple-length-scale deformation analysis in a thermoplastic polyurethane. Nat Commun 6, 6583. https://doi.org/10.1038/ncomms7583.

Sui, T., Salvati, E., Zhang, H., Dolbnya, I.P., Korsunsky, A.M., 2019. Multiscale synchrotron scattering studies of the temperature-dependent changes in the structure and deformation response of a thermoplastic polyurethane elastomer. Mater Today Adv 4. https://doi.org/10.1016/j.mtadv.2019.100024.

Tatai, L., Moore, T.G., Adhikari, R., Malherbe, F., Jayasekara, R., Griffith, I., Gunatillake, P.A., 2007. Thermoplastic biodegradable polyurethanes: The effect of chain extender structure on properties and in-vitro degradation. Biomaterials 28, 5407–5417. https://doi.org/10.1016/j.biomaterials.2007.08.035.

C.T. Thorpe, H.R. Screen, Metabolic Influences on Risk for Tendon Disorders, in: Ackermann, P., Hart, D. (eds), Metabolic Influences on Risk for Tendon Disorders. Advances in Experimental Medicine and Biology, (2016), 920. Springer, Cham. Doi: 10.1007/978-3-319-33943-6.

Tuan Ho, S., Hutmacher, D.W., 2006. A comparison of micro CT with other techniques used in the characterization of scaffolds. Biomater 27, 1362–1376. https://doi.org/10.1016/j.biomaterials.2005.08.035.

Walden, G., Liao, X., Donell, S., Raxworthy, M.J., Riley, G.P., Saeed, A., 2017. A Clinical, Biological, and Biomaterials Perspective into Tendon Injuries and Regeneration. Tissue Eng. Part. B Rev. 23, 44–58. https://doi.org/10.1089/ten.TEB.2016.0181.

Wendels, S., Avérous, L., 2021. Biobased polyurethanes for biomedical applications. Bioact Mater 6, 1083–1106. https://doi.org/10.1016/j.bioactmat.2020.10.002.

Yadav, P., Beniwal, G., Saxena, K.K., 2021. A review on pore and porosity in tissue engineering. Mater. Today: Proc. 44, 2623–2628. https://doi.org/10.1016/j.matpr.2020.12.661.

Yolcu, Ü., Alan, H., Malkoç, S., Bozkurt, Ş.B., Hakki, S.S.J., 2015. Cytotoxicity Evaluation of Bioresorbable Fixation Screws on Human Gingival Fibroblasts and Mouse Osteoblasts by Real-Time Cell Analysis. J. Oral Maxillofac. Surg. 73 (1562), e1–e. https://doi.org/10.1016/j.joms.2015.03.067.

Yudistira, A., Risantoso, T., Asmiragani, S., Basunanda, T.A., Putera, M.A., 2020. Combination of chondroitin sulfate and hyaluronic acid increases amount of fibroblast, collagen and decreases adhesion of achilles tendon after repair. J. Arthrosc. Jt. Surg. 7, 211–215. https://doi.org/10.1016/j.jajs.2020.06.002.

Zhou, G., Zhang, B., Tang, G., Yu, X.-F., Galluzzi, M., 2021. Cells nanomechanics by atomic force microscopy: focus on interactions at nanoscale. Adv Phys-X 6. https://doi.org/10.1080/23746149.2020.1866668.